Supporting Information

Synergistic Na-Site Ca and TM-Site Cu Doping in O3-Type $NaNi_{1/3}Fe_{1/3}Mn_{1/3}O_2$ Cathode towards Fast Kinetics and Long-Life Sodium-Ion Batteries

Chong Ye[1], Yilong Luo[1], Jiahao Chen[1], Huihua Min[2], Xinyuan Wu[1], Xiaomin Liu[1]*, Hui Yang[1,3]**

[1] College of Materials Science and Engineering, Nanjing Tech University, Nanjing 211816, Jiangsu, China

[2] Electron Microscope Lab, Nanjing Forestry University, Nanjing 210037, Jiangsu, China

[3] Micro-Nano (Ningbo) Electronic Materials Co., Ltd, Ningbo 315201, Zhejiang, China

* E-mail address: Liuxm@njtech.edu.cn

** E-mail address: yanghui@njtech.edu.cn

Section S1. Experimental Details

This Supporting Information presents a detailed description of the experimental procedures that complement the manuscript. It provides comprehensive information on the additional materials employed, complete characterization protocols, and electrochemical measurement techniques. These details are included to ensure the reproducibility of the experiments and to offer thorough understanding of the methodologies adopted in this work.

S1.1 Materials

Hydroxide precursor $Ni_{1/3}Fe_{1/3}Mn_{1/3}(OH)_2$ (GEM New Materials Co., Ltd.) was acquired commercially and employed as received without further purification. Na_2CO_3 (AR, 99.8%), $Ca(OH)_2$ (AR, 95%), $Cu(CH_3COO)_2 \cdot H_2O$ (AR, 98%) were purchased from Shanghai Lingfeng Chemical Reagent Co., Ltd. and used without further purification.

S1.2 Materials Characterization

Crystal structure was analyzed by X-ray diffraction (XRD, Rigaku Ultima IV 3 kW) with Cu Kα radiation (λ = 1.5406 Å, scan rate = 2° min^{-1}, scan range 10°−80°), and the lattice parameters of the unit cell were obtained by Rietveld refinement through the software of GSASII. The surface morphology and element distribution of the prepared cathode were characterized by Field Emission scanning electron microscopy (FESEM, JEOL, JSM-7100F). The spacing of crystal plane was further studied by high-resolution transmission electron microscopy (HR-TEM, JEM-F200). The chemical state of the

elements on the cathode surface was characterized by X-ray photoelectron spectroscopy (XPS, Thermo Fisher K-Alpha).

S1.3 Electrochemical Measurement

The electrochemical performance of all the synthesized cathode materials was studied through CR2032 coin-type half-cells. To fabricate the working electrode, the active substance, binder (polyvinylidene fluoride) and conductive agent (super-p) were mixed (mass ratio = 8:1:1) in N-methyl-2-pyrrolidone (NMP) solvent to prepare slurry. The slurry was then coated on aluminum foil and vacuum-dried overnight at 70℃. The dried electrodes were then cut into 13 mm diameter discs and transferred to a glove box under Ar atmosphere (H_2O < 0.1 ppm, O_2 <0.1 ppm) to assemble coin cells. Sodium metal was used as the counter electrode, a Whatman GF/D glass fiber membrane served as the separator, and the electrolyte was composed of 1 M $NaClO_4$ dissolved in a mixture of ethylene carbonate (EC) and propylene carbonate (PC) 1:1 (v/v), and 5 vol% fluoroethylene carbonate (FEC) as an additive. Galvanostatic charge-discharge (GCD) cycling was performed between 2.0 V to 4.0 V (vs Na/ Na^+) at 25 °C. Galvanostatic intermittent titration (GITT) was conducted on a Neware Battery Tester (Shenzhen, China). Rate capability was evaluated at various current densities. Electrochemical impedance spectroscopy (EIS) was performed using a CHI660e electrochemical workstation between 0.01 Hz and 100 kHz at the open circuit voltage. Cyclic voltammetry (CV) was tested on the LAND at a scan rate of 0.1 mV s^{-1} within the range of 2.0 V to 4.0 V (vs. Na/Na^+).

Section S2. Results and discussion Details

In this section, the equations and derivation procedures related to CV tests under various scan rates and GITT measurements are presented for clarity.

The formula of b-value test and Dunn method are as follows:

$$i_p = av^k \quad (1)$$

Equation (1) can be expressed as $\log(i_p) = \log(a) + k\log(v)$, where v represents the scan rate, i_p is the peak current, and k is the slope of $\log(i_p)$ versus $\log(v)$. Faradaic diffusion reactions and pseudocapacitive reactions are two distinct charge storage mechanisms in metal-ion batteries, and the magnitude of k indicates the control step. When k = 0.5, the reaction process is entirely dominated by Faradaic diffusion; when k = 1.0, the reaction process is entirely driven by pseudocapacitive effects.

$$i(V) = k_1 v + k_2 v^{1/2} \quad (2)$$

In **equation (2)**, k_1v represents the pseudocapacitive contribution and $k_2v^{1/2}$ corresponds to the diffusion-controlled contribution.

The diffusion coefficient of Na^+ can be calculated through GITT according to the following equation:

$$D_{Na^+} = \frac{4}{\pi\tau}\left(\frac{n_B V_m}{S}\right)^2\left(\frac{\Delta E_s}{\Delta E_\tau}\right)^2\left(\tau \ll \frac{L^2}{D_{Na+}}\right) \quad (3)$$

In equation (3), D represents the surface diffusion coefficient, τ represents the charge/discharge time per step of 600 s, and S represents the electrode area of 1.32 cm^2. M_B, m_B, V_M, and L represent the molar mass, molar volume, active material

content, and electrode thickness of the electrode, respectively. ΔEs and $\Delta E\tau$ denote the equilibrium potential difference and voltage change during the current pulse process.

Section S3. Supplementary Figures and Table

Supplementary figures (**Figure S1–S10**) and table (**Table S1**) are provided to support and further illustrate the electrochemical and structural characterizations discussed in the main text.

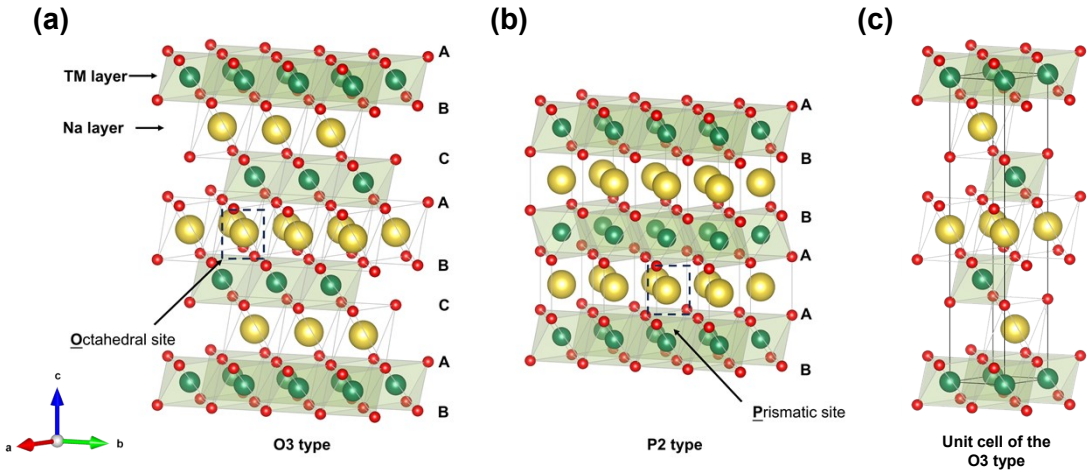

Figure S1. Schematic diagram of the crystal structure of (a) O3 type; (b) P2-type; (c) unit cell of the O3 type.

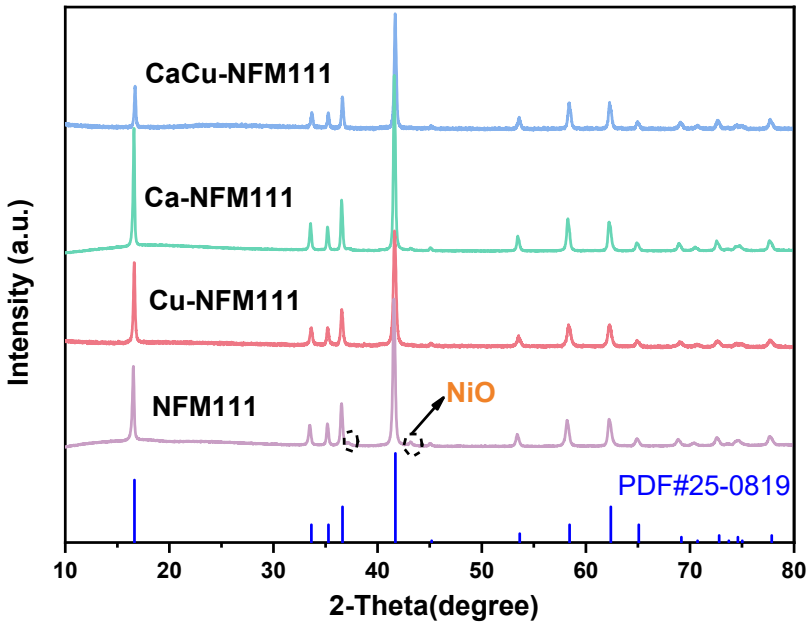

Figure S2. XRD patterns for NFM111, Ca-NFM111, Cu-NFM111 and CaCu-NFM111.

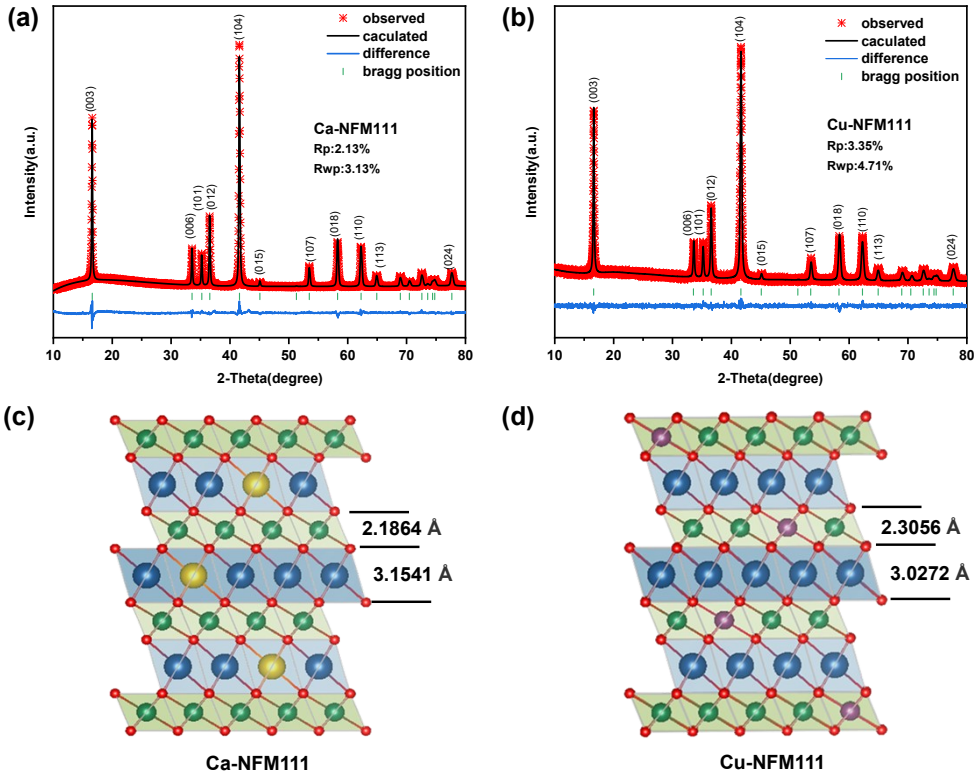

Figure S3. XRD Rietveld refinement of (a) Ca-NFM111 and (b) Cu-NFM111; Crystallographic structure of (c) Ca-NFM111 and (d) Cu-NFM111.

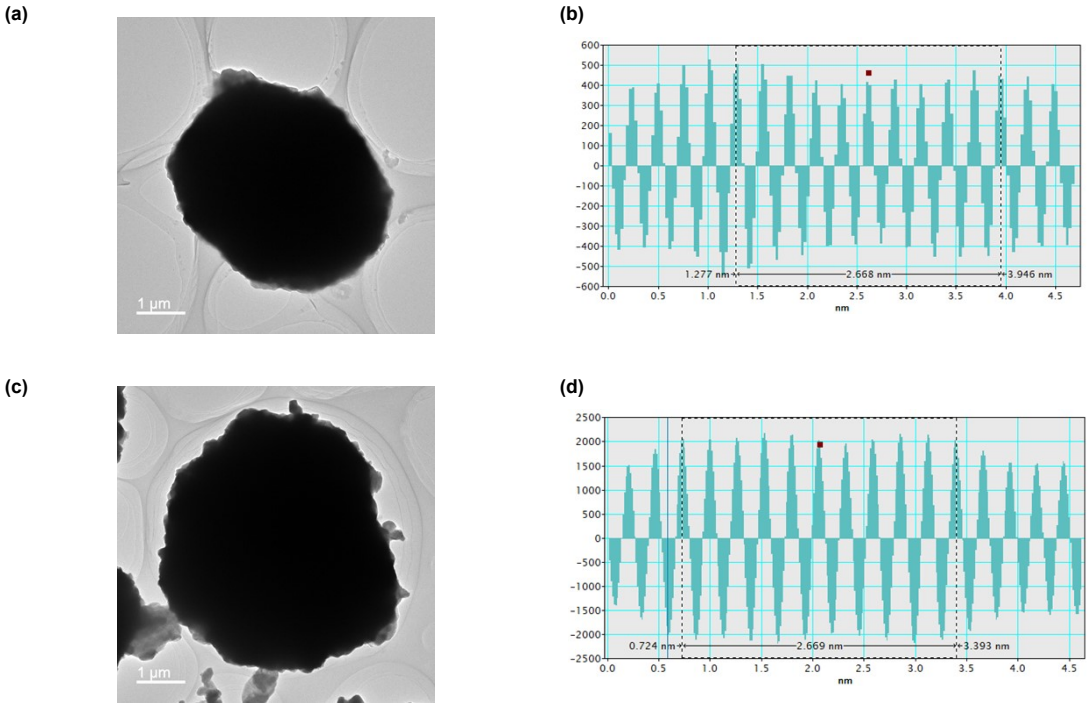

Figure S4. TEM image of (a) NFM111 and (c)CaCu-NFM111； lattice fringe spacing calculation of (b)NFM111 and (d)CaCu-NFM111.

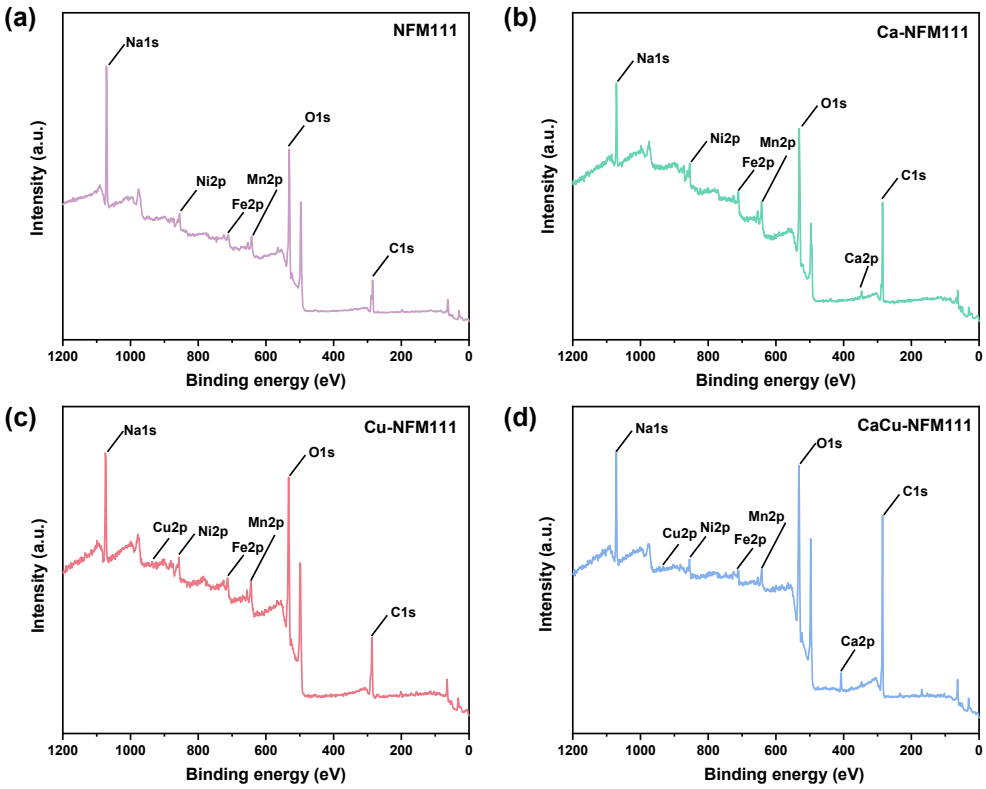

Figure S5. XPS survey spectra of (a) NFM111, (b) Ca-NFM111, (c) Cu-NFM111 and (d) CaCu-NFM111.

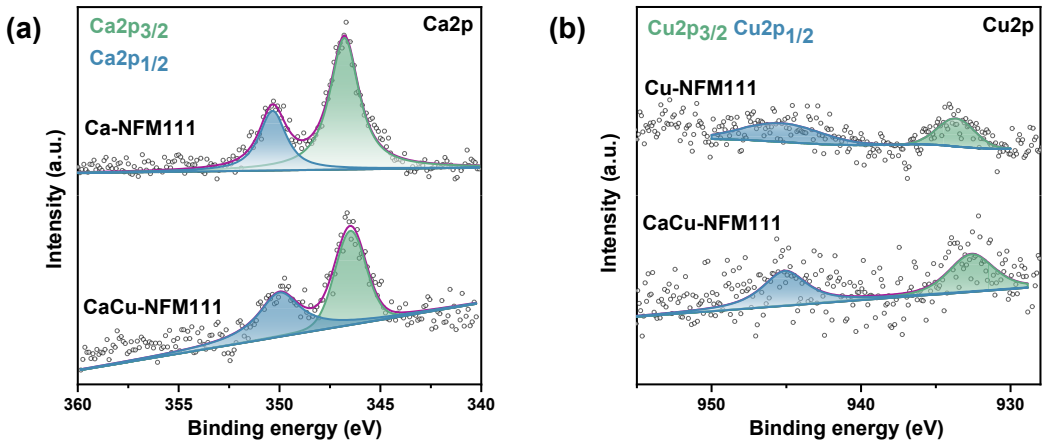

Figure S6. XPS spectra of Ca-NFM111, Cu-NFM111, CaCu-NFM111. (a) Ca 2p, (b) Cu 2p.

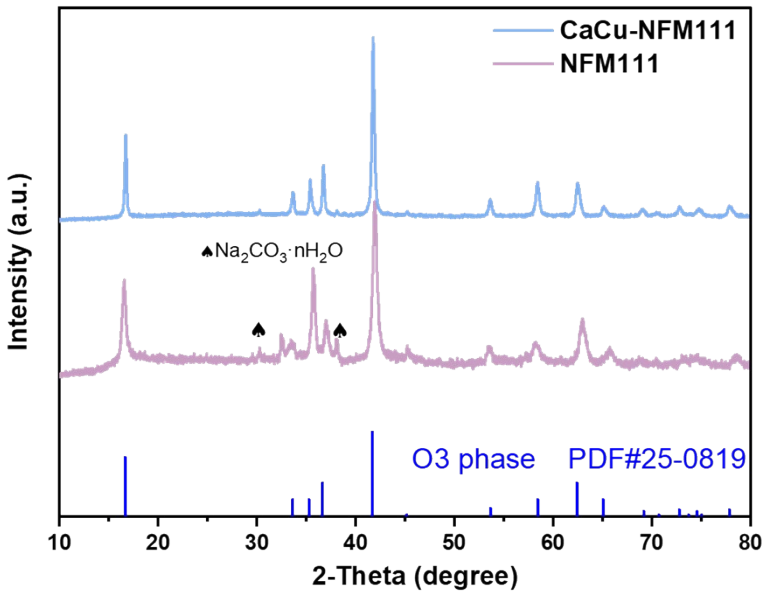

Figure S7. XRD patterns of NFM111 and CaCu-NFM111 after air exposure for one month.

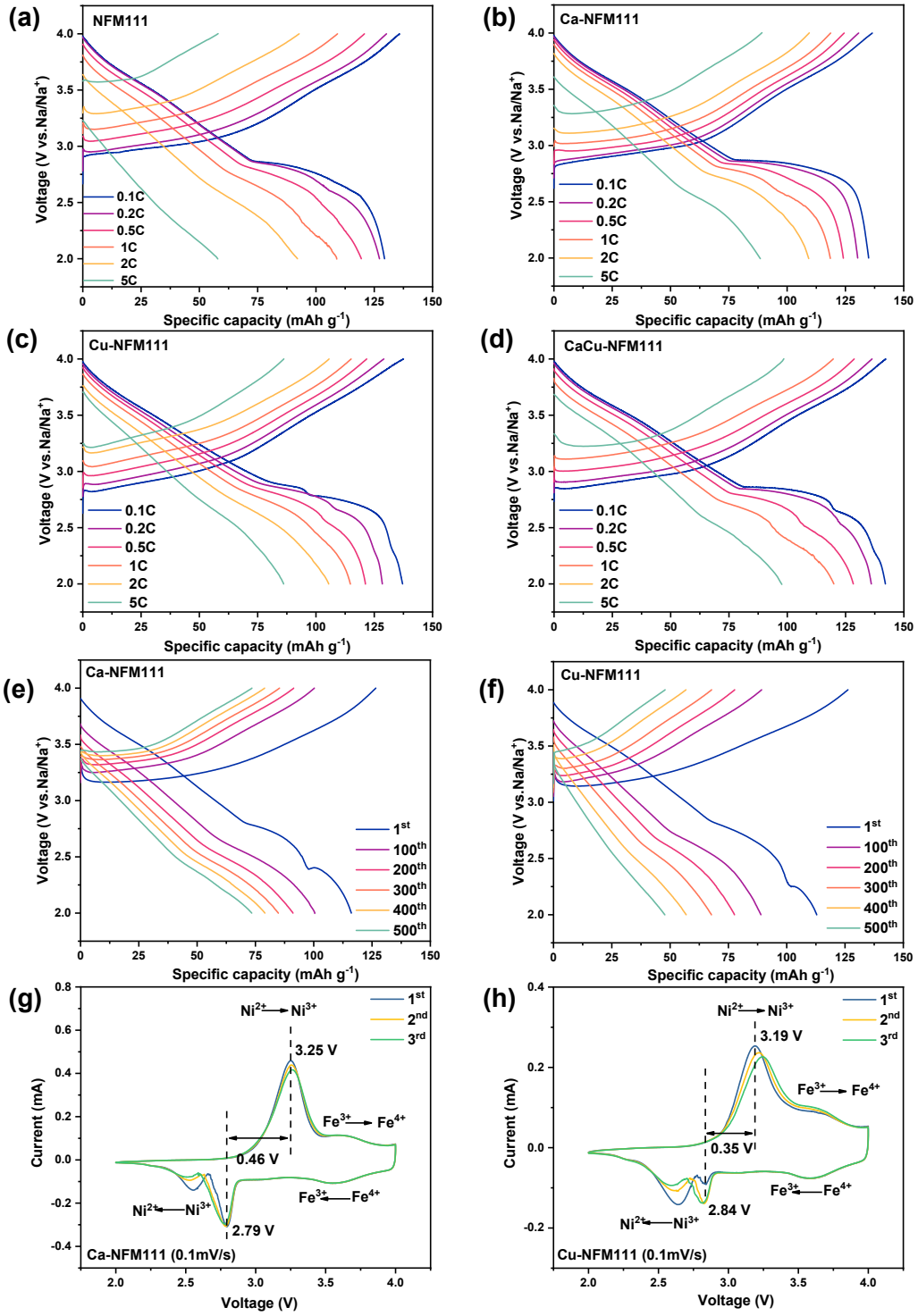

Figure S8. Charge/discharge curves at 0.1, 0.2, 0.5, 1, 2, 5 C for rate performance of (a) NFM111, (b) Ca-NFM111, (c) Cu-NFM111, (d) CaCu-NFM111. Charge/discharge curves of (e) Ca-NFM111, (f) Cu-NFM111 at 1 C. CV curves of (g) Ca-NFM111, (h) Cu-NFM111.

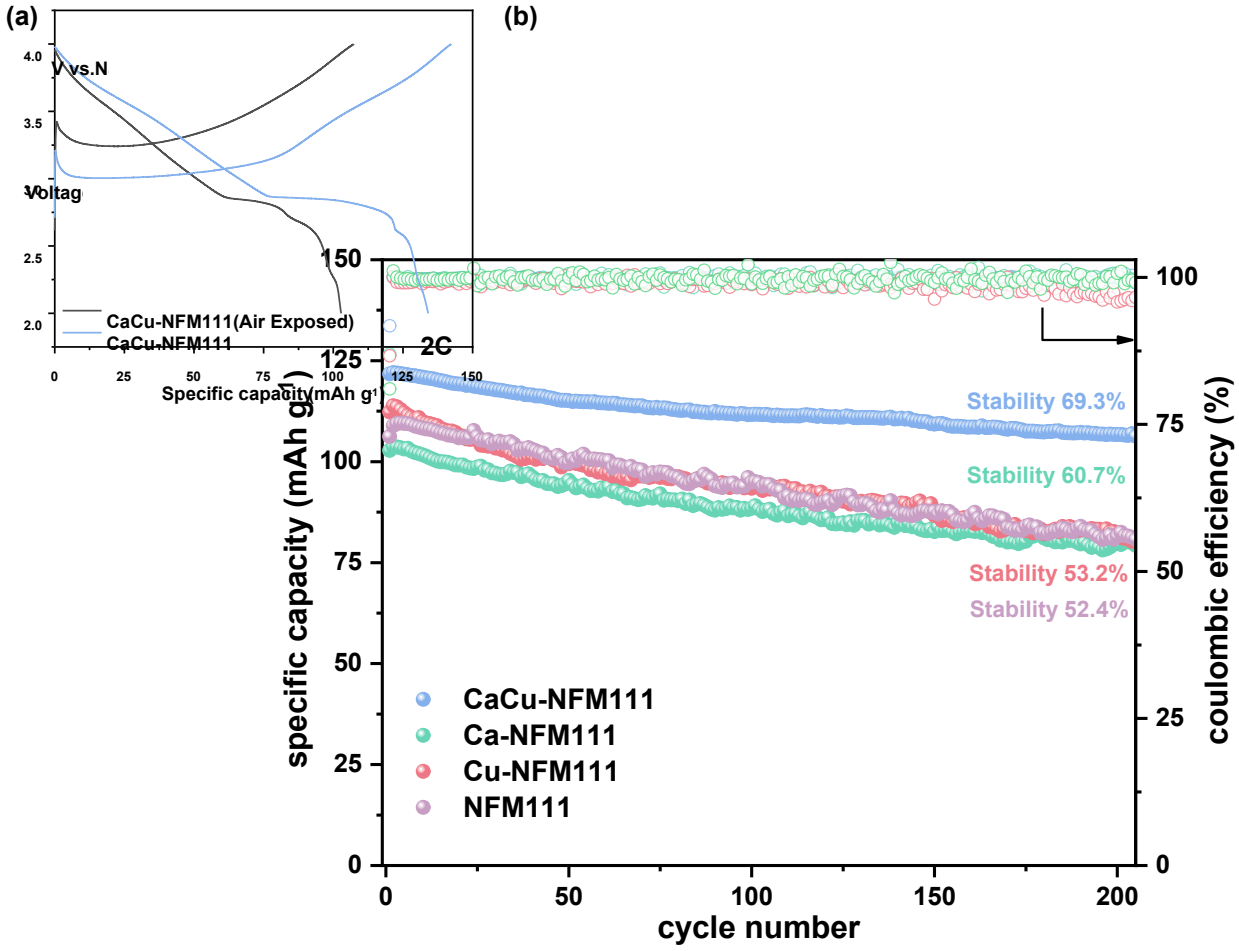

Figure S9. Cycling performance at 2 C.

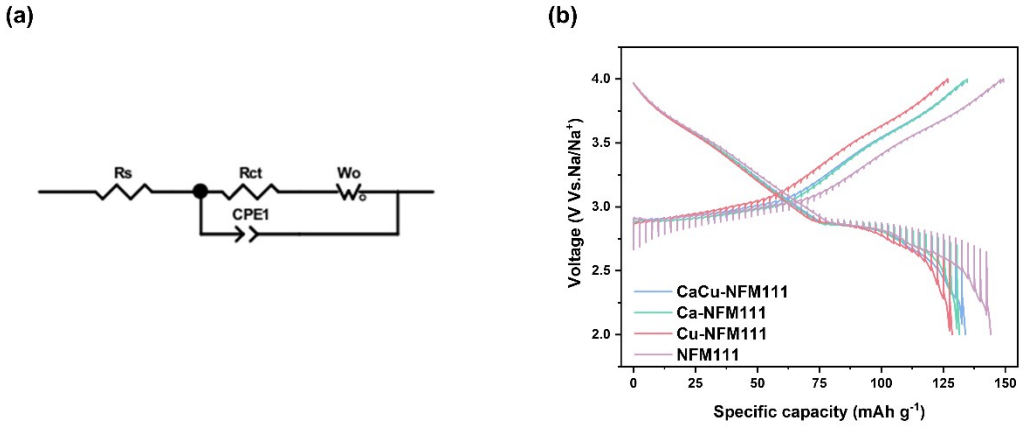

Figure S10. (a) Equivalent circuit diagram of fresh batteries. (b) GITT curves of NFM111, Ca-NFM111, Cu-NFM111, CaCu-NFM111.

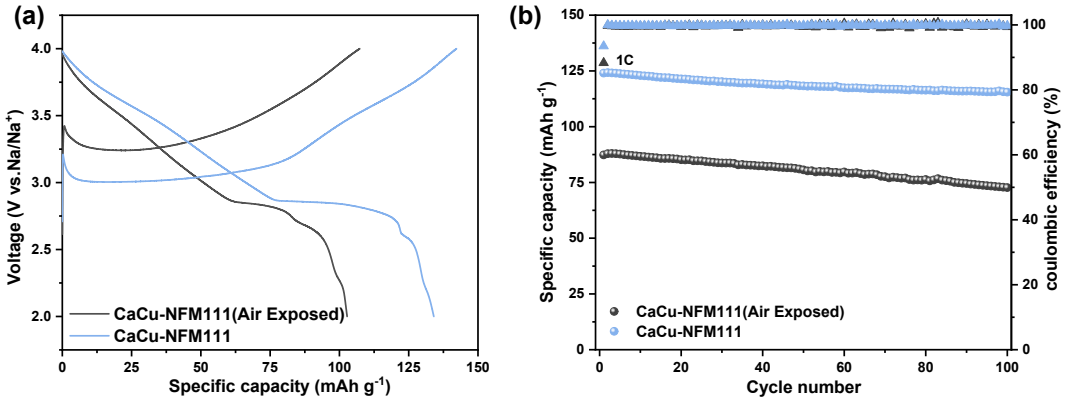

Figure S11. CaCu-NFM111 stored in air for one month (a) initial charge/discharge curves at 0.1 C, (b)Cycling performance at 1 C.

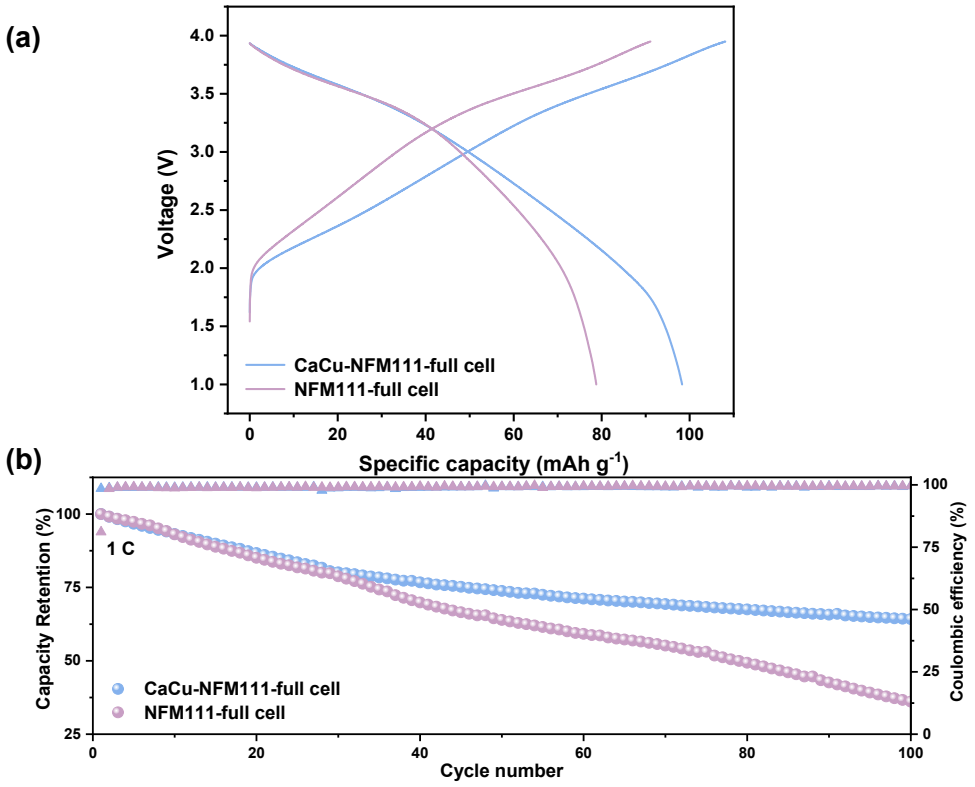

Figure S12. NFM111//Hard Carbon and CaCu-NFM111//Hard Carbon full cell (a) charge/discharge curves in the 1st cycle (b) capacity retention at 1 C.

Table S1. Structural refinement data for NFM111, Ca-NFM111, Cu-NFM111, CaCu-NFM111.

Samples	NFM111	Ca-NFM111	Cu-NFM111	CaCu-NFM111
***a* (Å)**	2.9812(8)	2.9811(6)	2.9817(29)	2.9862(25)
***c* (Å)**	16.0056(5)	16.0214(4)	15.9955(8)	16.0177(6)
***V* (Å^3)**	123.1930(5)	123.3054(31)	123.1600(19)	123.3020 (15)
c/a	5.3688	5.3743	5.3644	5.3732
Na-O length(Å)	2.3291(19)	2.3344(15)	2.3256(15)	2.3295(24)
Z_{OX}	0.2647(18)	0.2651(14)	0.2644(14)	0.2647(22)
d(NaO_2) (Å)	3.1382	3.1541	3.1272	3.1405
d(TMO_2) (Å)	2.1970	2.1864	2.2052	2.1987

Annotation: TM layer spacing: $d(TMO_2) = 2c\left(\frac{1}{3} - Z_{ox}\right)$; Na layer spacing: $d(NaO_2) = \frac{c}{3} - d(TMO_2)1$.

Reference

1. M. Li, H. Zhuo, J. Lei, Y. Guo, Y. Yuan, K. Wang, Z. Liao, W. Xia, D. Geng, X. Sun, J. Hu and B. Xiao, *Nat Commun*, 2025, **16**, 2010.